

Article

# $\delta^{13}\text{C}$ and $\delta^{18}\text{O}$ Stable Isotope Analysis Applied to Detect Technological Variations and Weathering Processes of Ancient Lime and Hydraulic Mortars

Elissavet Dotsika <sup>1,2,\*</sup> , Dafni Kyropoulou <sup>1,3</sup>, Vassilios Christaras <sup>1,3</sup> and Georgios Diamantopoulos <sup>1</sup>

<sup>1</sup> Institute of Nanosciences and Nanotechnology, Stable Isotope Unit, National Centre for Scientific Research, Demokritos, Agia Paraskevi, 15310 Attiki, Greece; d.kyropoulou@inn.demokritos.gr (D.K.); christar@auth.gr (V.C.); g.diamantopoulos@inn.demokritos.gr (G.D.)

<sup>2</sup> Institute of Geosciences and Earth Resources, Via G. Moruzzi 1, 56124 Pisa, Italy

<sup>3</sup> School of Geology, Faculty of Sciences, Aristotle University of Thessaloniki, GR-541 Thessaloniki, Greece

\* Correspondence: e.dotsika@inn.demokritos.gr

Received: 18 July 2018; Accepted: 4 September 2018; Published: 8 September 2018



**Abstract:** Samples of mortars were collected from lime and hydraulic mortars affected by environmental degradation. A total of 63 samples were obtained from Hellenistic, Late Roman and Byzantine historic constructions located at Kavala, Drama and Makrygialos in North Greece. Samples were collected in sections from the surface up to 6 cm deep using a drill-core material. The first sample was collected from the external layer, while the internal samples were collected each 1 cm deeper from the previous, in order to monitor the moisture ingress. Isotopic data will make it possible to create an ideal Hellenistic and Byzantine mortar layer and to provide weathering gradients. The isotopic values comprise a range of  $\delta^{13}\text{C}$  and  $\delta^{18}\text{O}$  values from  $-17.1\text{‰}$  to  $1.2\text{‰}$  and  $-25.9\text{‰}$  to  $-2\text{‰}$ , respectively. The weathering process of Hellenistic and Byzantine are expressed, by the regression lines  $\delta^{18}\text{O}_{\text{calcite matrix}} = 0.6 \times \delta^{13}\text{C}_{\text{calcite matrix}} - 1.9$  and  $\delta^{18}\text{O}_{\text{calcite matrix}} = 0.6 \times \delta^{13}\text{C}_{\text{calcite matrix}} - 2.0$  for hydraulic and Lime mortars respectively. Pronounced isotopic shift to heavy or light  $\delta^{13}\text{C}$  and  $\delta^{18}\text{O}$  in the carbonate matrix was attributed to the primary source of  $\text{CO}_2$  (atmospheric versus biogenic) and  $\text{H}_2\text{O}$  (evaporation of local primary water), in residual limestone and in secondary processes such as recrystallization of calcite with pore water and salts attack. Exogenic processes related to biological growth are responsible for further alterations of  $\delta^{18}\text{O}$  and  $\delta^{13}\text{C}$  in lime mortars. This study indicated that stable isotope analysis is an excellent tool to fingerprint the origin of carbonate, the environmental setting conditions of mortar, origin of  $\text{CO}_2$  and water during calcite formation and to determine the weathering depth and the potential secondary degradation mechanisms.

**Keywords:** stable isotopes;  $\delta^{13}\text{C}$ ;  $\delta^{18}\text{O}$ ; mortars; mineralogy; degradation

## 1. Introduction

It is very important to respond to major new challenges regarding the conservation of cultural heritage, by predicting deterioration features and evaluating the nature of damages monuments. Its preservation demonstrates recognition of the necessity of the past while on a different level ensures a mean for the validation of human-memories and confirms human history. The material nature of monuments is what makes it so important, allowing a direct interaction with human senses, yet it also entails that it is a constant state of chemical transformation, making its preservation an everlasting task of continuously growing importance. Hydraulic and lime mortars constitute main structural components in architectural constructions. Environmental degradation of historic mortars are a main threat for the preservation of historic monuments [1–6]. The main agents of decay (such as acid

attack, leaching action, salts attack, damage due to frost and fire, insufficient mixing and choice of constituents) can cause extensive cracks and total disintegration of historic constructions [7–10]. There are two main categories of limes, hydraulic and non-hydraulic. Lime is formed by burning a source of calcium carbonate such as limestone to evolve carbon dioxide and form calcium oxide (1) [(CaO, quicklime)]. The calcium oxide is then slaked with water under heating to produce calcium hydroxide (slaked lime, Ca(OH)<sub>2</sub>) (2). This mass will be then mixed with aggregate materials such as sand, gravel, crushed stone or iron blast-furnace slag and various organic and inorganic additives such as pozzolanic materials or mud, forming calcium carbonate (3). The mortar hardens with the absorption of carbon dioxide from the atmosphere gaining strength. The formation of calcium carbonate mortars is described in the following reactions:

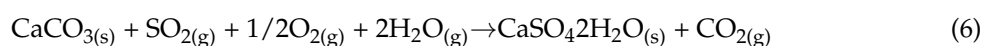


The reactions within the formation of hydraulic compounds are described below:



The sources of mortar decay could be physical, related to physical variations of water inside masonry (evaporation, capillary flow, ice formation, etc.) or chemical (formation of expansive products such as ettringite and thaumasite).

Also, lime-based mortars can be easily attacked by sulphur compounds. Sulfation occurs when a layer of gypsum is formed in the surface of calcite that is more soluble than calcite (6).



Therefore, in the presence of water (rain) this gypsum layer is dissolved, causing dissolution of the external calcite layer. Furthermore, concrete deterioration can be related to internal sulfate attack. Aggregates containing sulfide minerals (pyrite) can become an internal source of sulfate ions. These ions can promote the development of chemical reactions with the cement paste composition, which may result in the formation of expansive and deleterious products that are typical of sulfate attack known as ettringite, gypsum and thaumasite [11,12].

In order to determine the above degradation mechanisms and propose suitable conservation strategies, it is essential to examine the calcium carbonate origin and to identify the possible causes that changed the initial composition. Stable isotopic data provides information of the primary sources of raw material and offers considerable potential in the investigation of lime mortar and lime plaster (composed of sand, water, and lime and often contained horse hair for reinforcement and pozzolan additives). In particular, stable isotope fingerprinting is a concept that has been successfully developed and applied in earth sciences for several decades [13,14]. The elements C and O have a characteristic isotope ratio that varies slightly but significantly when transformations like phase changes or chemical reactions occur. Those slight variations can be measured and allow for valuable conclusions to be drawn on the origin and the history of these elements. Previous studies on historical mortars implemented mineralogical and chemical analysis, evaluation of the aggregate to matrix ratio and provenance of raw materials [15–18]. However, studies focused on stable isotope analysis of lime mortars are rare [19,20]. Furthermore, little is known about the isotopic change of the initial C and O in carbonate matrix that was caused by alteration of the primary source of CO<sub>2</sub> and H<sub>2</sub>O in mortar over time. Human influence and biological growth are major exogenic processes which alter O and C in lime mortar. In particular oxygen isotope is common between CO<sub>2</sub> and H<sub>2</sub>O and has the potential to elucidate the

history of primary source of H<sub>2</sub>O or alteration processes with water of meteoric origin, while carbon isotope composition can identify the origin of CO<sub>2</sub>. Finally, the main objective of this study is to examine the sources of mortar decay in four Hellenistic, Roman, Late Roman and Byzantine masonries. The determination of the exact origin of the materials is the key to reach the above objective and this can be achieved using stable isotopes. Furthermore, stable isotope analysis will allow examining what has changed relatively to environmental conditions and secondary processes from ancient time until today, to distinguish the nature of the structural materials used (mortar) and to disambiguate the causes that incurred the degradation phenomena.

## 2. Methods and Materials

### 2.1. Methods

Mortar lumps were analyzed using Scanning Electron Microscopy (SEM) with Energy Dispersive X-ray (EDX) analysis since this technique is considered a powerful tool to characterize the microstructure of the materials [21,22].

Major and minor elements for polished mortar samples were analyzed using a FEI/Quanta Inspect D8334 SEM, FEI company, Hillsboro, OR, USA, fitted with a low vacuum chamber and an energy dispersive X-ray analyzer at NCSR “Demokritos”, Athens, Greece. The operating conditions were a 25 KV accelerating potential and a 107 µA emission current, giving a count rate of 400 cps on metallic cobalt, the working distance was normally 10 mm. The detector was calibrated with a range of pure elements, synthetic oxides and well characterized minerals. The mortar samples were vacuum-dried, polished in resin blocks, mounted onto metal stubs and coated with a thin film of gold and examined with the SEM.

The elements present in the mortar samples were determined using X-ray measurements of each particle. A backscattered electron image was obtained in every sample and qualitative analysis of 10–20 individual particles was performed. For bulk analysis of mortars, the SEM beam was rastered on each sample at 100× over a 4 × 3 mm sized area. Accuracy and precision in bulk analysis for mortar samples were expected to be somewhat reduced because mortars are heterogeneous materials, however for comparative purposes the results were normalized to 100% and are considered to give an approximation of the major oxides. The imaging was performed using four-quadrant Backscattered Electron Imaging (BSE). The backscattered images enabled the determination of the structural components in mortars, since heavy elements such as iron and lead appear brighter than light elements such as carbon or oxygen. As a result, backscattered electron images demonstrate the make-up of mortars, because sharp changes in grey levels represent different compounds.

Mineralogical analysis was achieved using optical microscopy [22,23]. Optical microscopy was performed using a polarizing microscope at the Department of Mineralogy, Petrology and Economic Geology at Aristotle University of Thessaloniki. Thin sections were prepared by drying the samples (lumps) using acetone in vacuum. The samples were vacuum impregnated with epoxy resin, cut with a slow-speed diamond saw to minimize damage and then mounted on glass slides and ground to 30 mm thickness. Observations were made under crossed polars (XPL) using a Leitz Laborlux 11 POL S, (Leica Microsystems’ Microscopy and Scientific Instruments, Wetzlar, Germany). The aggregate clasts, and the fine-grained calcite, may be identified using common geological techniques [24,25]. The terminology developed for the description of archaeological ceramics was applied to some extent in mortar cross section investigations [26,27].

The isotopic analyses took place at Stable Isotope Unit of Institute of Nanosciences and Nanotechnology (NCSR “Demokritos”) on a Thermo Delta V Plus IRMS equipped with GasBench II device. Mortar samples were separated using scalpels in two or three sections reflecting the changes in isotopic composition from interior to exterior. Small quantities of clean (leached with acetic acid) carbonate material were separated and after grinding to a fine powder were diluted in ortho-phosphoric acid and the CO<sub>2</sub> produced was measured in the isotope ratio mass spectrometer. The isotopic results

are reported in the usual delta terminology versus VPDB isotopic standard, delta being defined as follows:  $\delta = [(R_{\text{sample}} - R_{\text{standard}})/R_{\text{standard}}] \times 1000$  where R is the ratio between the heavy and the light isotope, in this case  $^{18}\text{O}/^{16}\text{O}$  or  $^{13}\text{C}/^{12}\text{C}$ . The reported values are the mean of two or more consistent measurements of each sample. The standard deviation of the materials measurements is very good, ranging on average between  $\pm 0.1\text{‰}$  and  $\pm 0.2\text{‰}$  [28–30].

## 2.2. Materials

A total of 63 samples were obtained from four Hellenistic, Late Roman and Byzantine historic constructions located at Kavala, Drama and Makrygialos in North Greece (Figure 1). The location of the studied sites is considered maritime therefore all the architectural constructions and all mortar samples are seriously affected by salt crystallization [31,32]. Also, extensive fragmentation is observed in fortification walls in Drama, in Marmarion tower in Kavala and in funerary monuments in Makrygialos. Different types of crust are also observed in the surface of the mortars. Dark soiling patterns are observed on the mortars surface. Black crusts are likely to be derived from secondary recrystallization of calcitic binders while green crusts are associated with biodegradation and biological growth. The samples were collected in sections by pressing a drill-core material 6 cm towards the surface. The first sample was collected from the surface, while the internal samples were collected each 1cm deeper from the previous. The samples collected from the exterior layers are exposed to environmental degradation while the samples collected from interior layers do not possess any evidence of degradation.

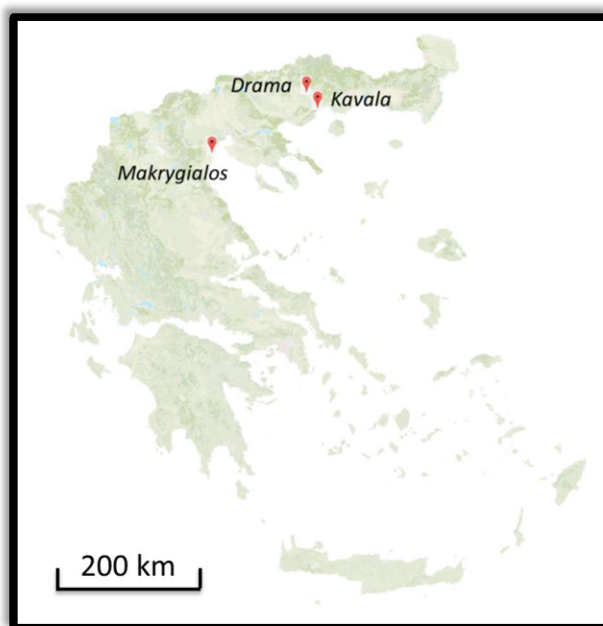


**Figure 1.** Map of sampling locations. Makrygialos ( $40^{\circ}25' \text{ N } 22^{\circ}36' \text{ E}$ ), Drama ( $41^{\circ}9' \text{ N } 24^{\circ}8' \text{ E}$ ), Kavala ( $40^{\circ}56' \text{ N } 24^{\circ}24' \text{ E}$ ).

### 2.2.1. Anaktoroupoli and Land Walls in Kavala

Samples (AN1a-1 to Anp-1) were obtained from Anaktoroupoli which is an area located in the region of Nea Peramos in Kavala, Greece. In specific, Anaktoroupoli is the remaining of a Byzantine town located in the west coast of Kavala. It is dated at 14th century AD based on the characteristics of the masonry and the features observed in the coins excavated in the region [33]. The samples collected from this site were joints. The joints of the brickwork structure are  $2 \pm 4$  cm thick, and probably have a bearing function [34]. A few samples were also collected from land walls in Kavala (KA1b, KA5 and KA6), but these were not included in stable isotope analysis, because of analytical errors (the samples

KA1b, KA5, KA6 were entirely covered with salt and the SEM detector could not detect the other constituents). Land walls in Kavala were constructed in four different historical periods; however samples selected were characterized as late Byzantine (9th to 10th century).

#### 2.2.2. Marmarion Tower in Kavala

Samples (MA1-3 to MA5-2) were collected from Marmarion tower in Kavala, Greece. The Marmarion tower was built in 1367 by Priests Alexios and Ioannis for the Ancient Monastery of Pantokratoras. The tower is constructed using secondary ancient material, mainly sandstones, marlstones, fired bricks and good quality lime mortar. The ancient material is composed of large marlstones from architectural parts such as inscribed columns [34].

#### 2.2.3. Fortification Walls in Drama

Samples (DRa-1 to DR2g-1) were obtained from joints located at fortification walls that surround the historical center of Drama, one of the most important monuments of the region [34]. Two main parts of the walls have survived: the northern parts have been almost entirely preserved, apart from the north-eastern corner and all of the west part. The walls were founded in Late Roman times (3th–6th century AD) and later building phases are ascribed to the Frankish period. Modern building materials were identified, added possibly within restoration treatments. This study will examine samples from the Later Roman building phase.

#### 2.2.4. Funerary Monuments in Makrygialos

Mortar samples (MK1-1 to MK10-2) were obtained from 4th century BC Hellenistic tombs in the area of Pydna in North Greece. Ancient Pydna lies in the North of Pieria, two kilometers away from South Makrygialos. The monuments were discovered in rescue excavations under the supervision of KZ' Ephoreia of Classical and Prehistoric Antiquities [35].

### 3. Results

#### 3.1. Micromorphological and Elemental Analysis

##### 3.1.1. Anaktoroupoli-Land Walls Kavala

Backscattered electron photomicrographs of sample AN1b, representative of the group of samples obtained from Anaktoroupoli, Nea Peramos, illustrates the morphology of a Byzantine mortar. The photomicrograph (Figure 2) depicts large irregularly shaped grains acting as aggregates, while the matrix is composed from homogeneous smaller grains. The sample is composed of 50.7% quartz and 31.7% CaO according to bulk analysis of oxides in the SEM and the ternary plot with EDX values (Table 1). Petrographic analysis elucidated that the matrix is composed of microcrystalline calcite (Figure 3). Thin section demonstrates that this is a coarse mortar, the size of mineral components rises up to 6 mm. The mineralogical composition of the aggregates in this sample includes quartz, calcite, plagioclase, potassium feldspar, microcline, muscovite and traces of sericite and kaolinite. Thin section photomicrograph indicates that quartz is the most abundant mineral, in line with SEM analysis; quartz grains reach up to 3 mm. Quartz is usually coarse and shows a strong recrystallization layer on the boundaries of quartz grains. Most of the mineral components demonstrate rounded cavities surrounded by a thin layer of calcite. Backscattered electron photomicrograph reveals fibrous crystals of sericite (indicated with black arrow) with hexagonal structure and needle morphology (10 mm in length) are present as parts of the aggregate fraction. Calcitic matrix shows intensive fragmentation and cracks attributable to the degradation of mortar over time. Extensive deposition of salts is observed in sample K5, obtained from land walls in Kavala. The surface of the mortar is entirely covered with salts. Point analysis detected the elements Na and Cl on the entire surface of the sample.

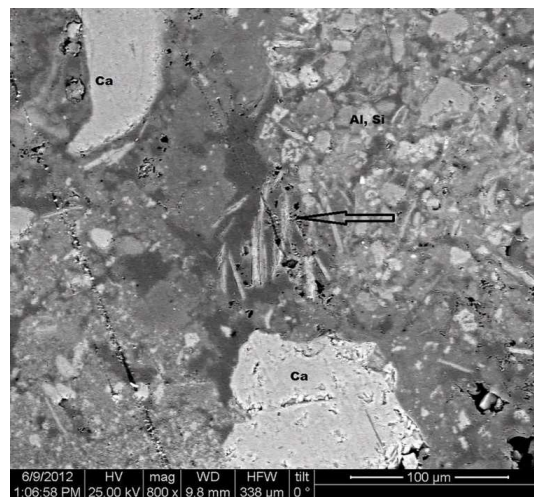


**Figure 2.** SEM/Backscattered Electron Imaging (BSE) ( $\times 253$ ) photomicrograph of sample AN1b from land walls in Kavala. The black arrow indicates fibrous crystals of sericite.

**Table 1.** Data in weight per cent oxide normalized to 100%.

Sample	Location	Al <sub>2</sub> O <sub>3</sub>	SiO <sub>2</sub>	CaO	MgO	Cl <sub>2</sub> O	K <sub>2</sub> O	Na <sub>2</sub> O	BaO	Fe <sub>2</sub> O <sub>3</sub>
AN1b	Anaktoroupoli, Kavala	10.4	50.7	31.7	na	0.6	3.2	2.4	na	na
DR2c	Drama	9.8	57.6	13.0	13.2	1.4	na	na	na	5.1
Dr3	Drama	3.5	49.0	49.0	1.3	1.1	na	na	na	na
KA1b	Land walls, Kavala	10.4	50.7	31.7	na	0.6	na	2.4	na	na
KA5	Land walls, Kavala	5.3	29.8	54.5	na	2.4	na	3.8	na	na
KA6	Land walls, Kavala	7.6	38.7	na	0.5	22.2	3.3	26.3	1.5	na
MA2	Marmarion Tower, Kavala	9.8	52.9	33.4	na	na	na	na	na	na
MA6	Marmarion Tower, Kavala	7	36.5	47.7	1.7	1.5	na	na	na	5.4
MK4	Makrygialos	6.2	58.7	29.7	1.2	na	0.7	0.5	na	1.5
MK5	Makrygialos	13.2	43.4	32.0	2.3	na	2.2	na	na	4.5
MK6	Makrygialos	4.8	23.9	65.0	1.2	na	2.3	na	na	1.1
MK7	Makrygialos	4.6	9.4	86.0	na	na	na	na	na	na
MK10	Makrygialos	na	4.4	95.6	na	na	na	na	na	na
MK11	Makrygialos	6.2	56.0	31.7	0.7	na	1.5	na	na	1
MK12	Makrygialos	5.3	30.0	60.2	1.0	na	1.0	na	na	1.6

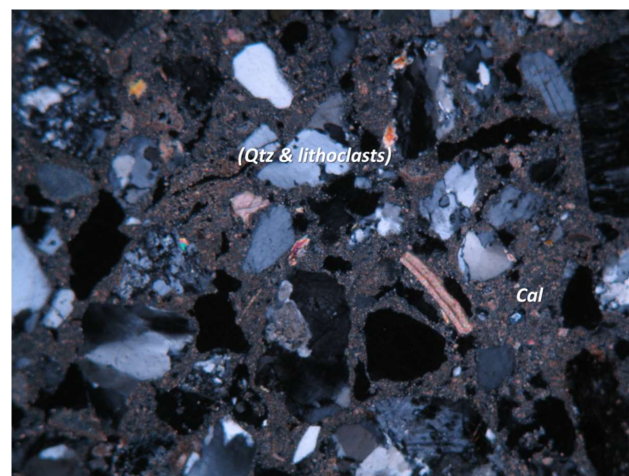


**Figure 3.** Crossed polar (XPL), magnification  $5 \times 5$  mm, photograph length 2 mm. Byzantine mortar AN1b. The binder is composed microcrystalline calcite while the aggregates are composed of quartz grains and lithoclasts in sedimentary petrology.

### 3.1.2. Fortification Walls in Drama

SEM-EDX microstructural observations and thin section analysis revealed the morphology of DR2c (Figure 4) representative sample from fortification walls in Drama. Bulk analysis of oxides (Table 1) with SEM demonstrates that mortar samples from Drama are composed of 13.0% CaO and 57.6% of SiO<sub>2</sub>. Point analysis of elements in each sample also revealed that Si occurred as the most abundant element in all SEM-EDX measurements. Minor elements detected were Al, Mg, Cl and Fe. Parallel to elemental analysis using SEM, thin section analysis in the polarized optical microscope demonstrates that the aggregates in the mortar samples from Drama are composed of quartz, calcite, plagioclase, potassium feldspar, biotite, muscovite with traces of granite, actinolite and tourmaline. The matrix is composed of fine grained calcite. When viewed in XPL sample DR2c has an overall brownish color, since this sample contains minerals and fragments of crushed bricks with maximum size 1 cm. Looking at photomicrograph (Figure 5), quartz demonstrates a coarse structure, at the same time appears a strong recrystallization matrix in saturation boundaries. XPL observations reveal the presence of muscovite together with quartz. The aggregate is formed from a pozzolanic additive of crushed and powdered ceramics plus a geological material such as volcanic rock with particles of variable composition. Muscovite is dispersed through calcitic binding material in the form of leaves with size up to 1mm. The presence of plagioclase is rare. Ceramic components are composed of muscovite, quartz and calcite. Elemental analysis also detected traces of chlorine in all samples, providing evidence for extensive deposition of salts. All samples demonstrate porous morphology that enhances the transportation of salts in the mortar structures using moisture. The black holes in the mortar structure are attributed to shrinkage within the polishing process and they do not represent evidence of porosity.

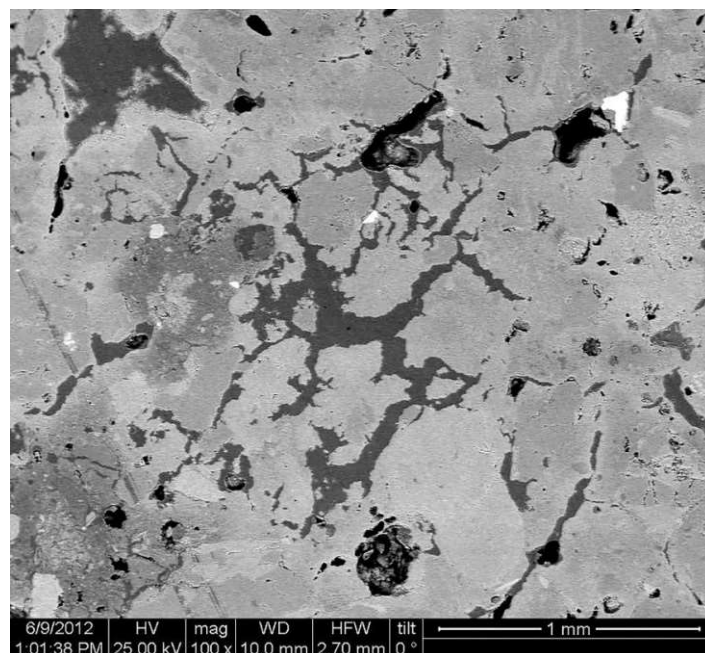


**Figure 4.** SEM/BSE ( $\times 253$ ) photomicrograph of sample DR2c from fortification walls in Drama. Microstructural observations and thin section analysis.

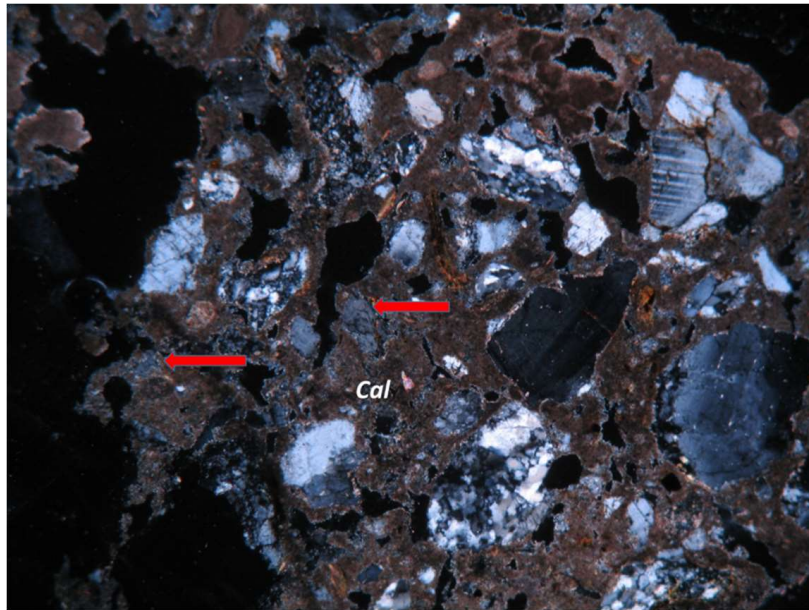


**Figure 5.** XPL, magnification  $13 \times 10$  mm, +N, photograph length 1mm. Byzantine mortar, DR2c from fortification walls in Drama. The binding material is composed of calcite, pozzolanic reactions are observed (the arrows indicate the reactions), crushed ceramics and rock fragments compose the aggregates.

### 3.1.3. Marmarion Tower—Kavala

SEM/BSE and XPL photomicrographs demonstrate the microstructure of sample MA3 representative of samples obtained from Marmarion tower in Kavala (Figures 6 and 7). Bulk analysis of oxides shows that this sample contains 47.73% of CaO and 36.54% of SiO<sub>2</sub>. Point analysis of individual elements showed that the aggregate is mostly composed of Si-rich particles while the matrix is composed of Ca-rich particles. The mineralogical composition of the matrix is detected using thin section analysis; the binding material is composed of fine-grained calcite. The aggregate can be readily discriminated from the matrix on the basis of its different mean atomic number, as shown in Figure 6. The aggregate is composed of quartz, calcite, plagioclase, potassium feldspar, microcline, biotite, muscovite while traces of chlorite were detected in the sample. XPL observations demonstrate that the length of quartz rises up to 2 mm and it is usually coarse. Quartz grains are surrounded by a strong recrystallization layer in the saturation boundaries. Calcite demonstrates intensive cracks and fragmentation, while signs of recrystallization layers are observed in a few samples. Elemental analysis also detected traces of Cl-rich particles in all samples, providing evidence for deposition of salts. All samples demonstrate porous morphology, which enhances the transportation of salts in the mortar structures using moisture.

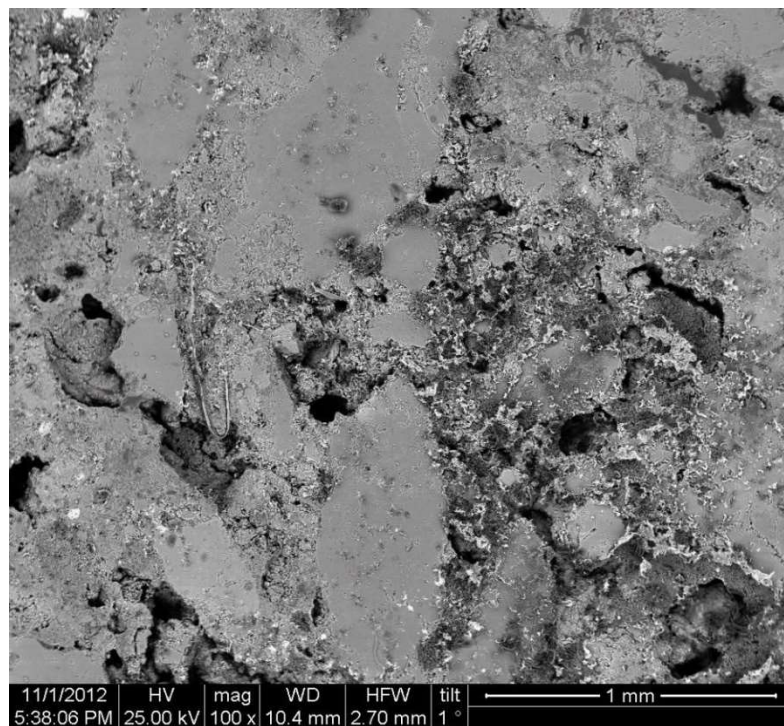


**Figure 6.** SEM/BSE ( $\times 300$ ) photomicrograph of sample MA3 obtained from Marmarion tower.

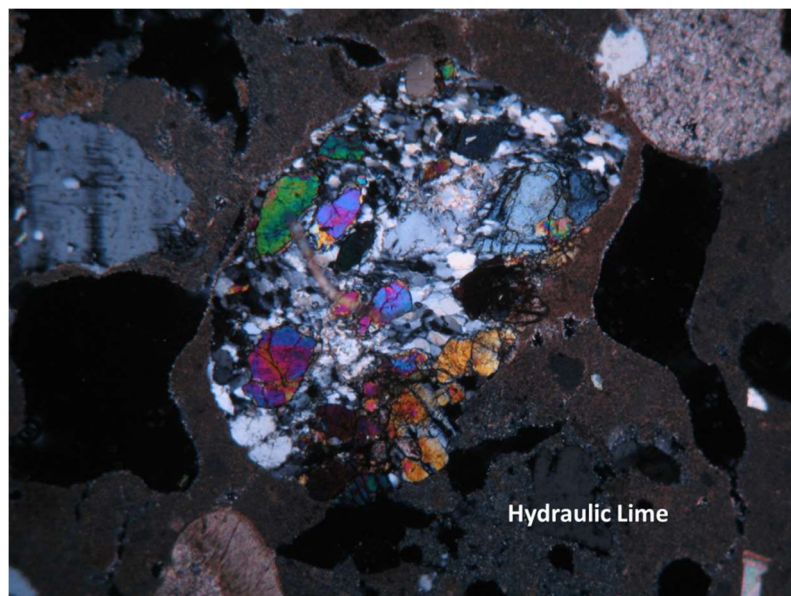


**Figure 7.** XPL, magnification  $6 \times 5$  mm, +N, photograph length 2 mm. Sample MA3 obtained from Marmarion tower, it is a typical lime pozzolan mortar.

#### 3.1.4. Makrygialos

Backscattered electron and XPL photomicrographs of sample MK4 (Figures 8 and 9), illustrate the morphology of typical mortar sample from Makrygialos, Greece. The photomicrographs (Figure 8a,b) depict large irregularly shaped lithoclast composed mainly of quartz (up to 58.7%) and feldspar, as shown by bulk analysis of oxides in the SEM (Figure 10). Petrographic observation elucidates that this is a textured mortar with mineral components sized from  $100 \mu\text{m}$  to 4 mm. The matrix is composed from fine calcitic particles including also quartz grains, bulk analysis of oxides detected

95.6% percentage of CaO (Table 1, Figure 10). The matrix is composed of micritic calcite that is interrupted by angular aggregates and pores. XPL observation demonstrated that the mineralogical composition of the aggregate is: microcrystalline calcite with quartz, plagioclase, orthoclase, microcline, biotite, muscovite and traces of chlorite, zircon, titanite. Volcanic grains are also observed. The size of quartz grains is approximately 2 mm. The black holes in the pictures (Figure 8a,b) are pores in the mortar structure. In this sample, it is possible to have two types of pores. The elongate cracks are attributed to shrinkage and the rounded pores are derived from bubbles during setting. In places where heating was more intense, the half-burnt limestone fragments show an edge along the area of a crack (pore) [(Figure 8b, indicated with yellow arrow)]. It represents deposition of calcite on the edge of the crack due to the movement of solutions during burial. Thin section analysis also reveals the presence of unreacted lime and rare particles of partially or unburned limestone. The black hole in Figure 8b is lined with a very light grey line composed of calcite. This pore lining requires a source of dissolved carbonate. The dissolved carbonate could be attributed to the dissolution of calcite matrix or dissolution of the calcitic particles in the aggregate. In sample MK4 the matrix is mostly composed of calcite, therefore the pore lining is attributed to the dissolution of calcite matrix. Fine calcite particles (indicated with black arrow) in the matrix is attributed to limestone relicts that are derived from insufficient burning.

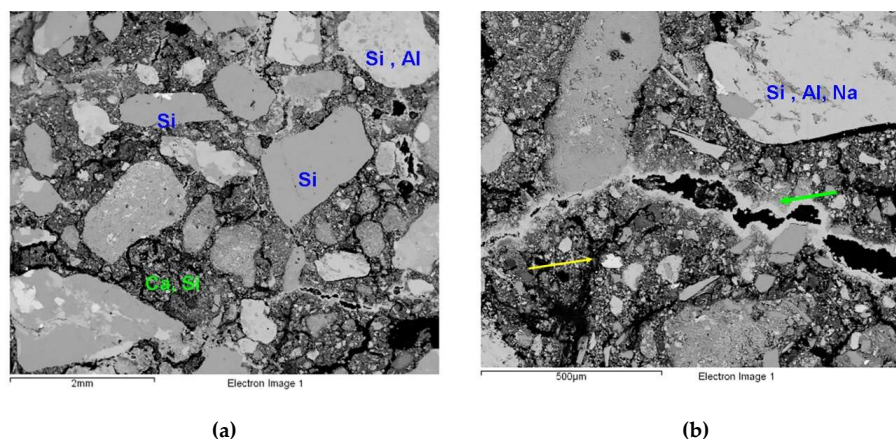


**Figure 8.** (a,b) SEM/BSE ( $\times 100$ ) photomicrographs of sample MK4 obtained from Makrygialos. The potential minerals are quartz (up to 58.7%) and feldspar. The matrix is composed mainly from calcite and quartz. The arrows in (b) indicate half-burnt limestone fragments.

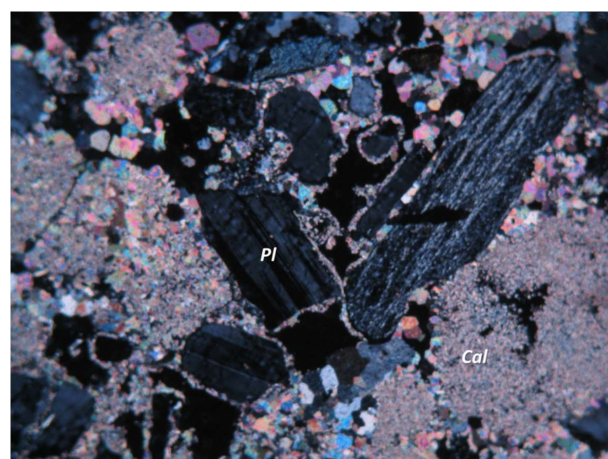


**Figure 9.** XPL, magnification  $1 \times 5$  mm, +N, photograph length 2 mm. Hellenistic mortar sample MK4 obtained from Makrygialos, Greece. Microcrystalline calcite and plagioclase as aggregates.

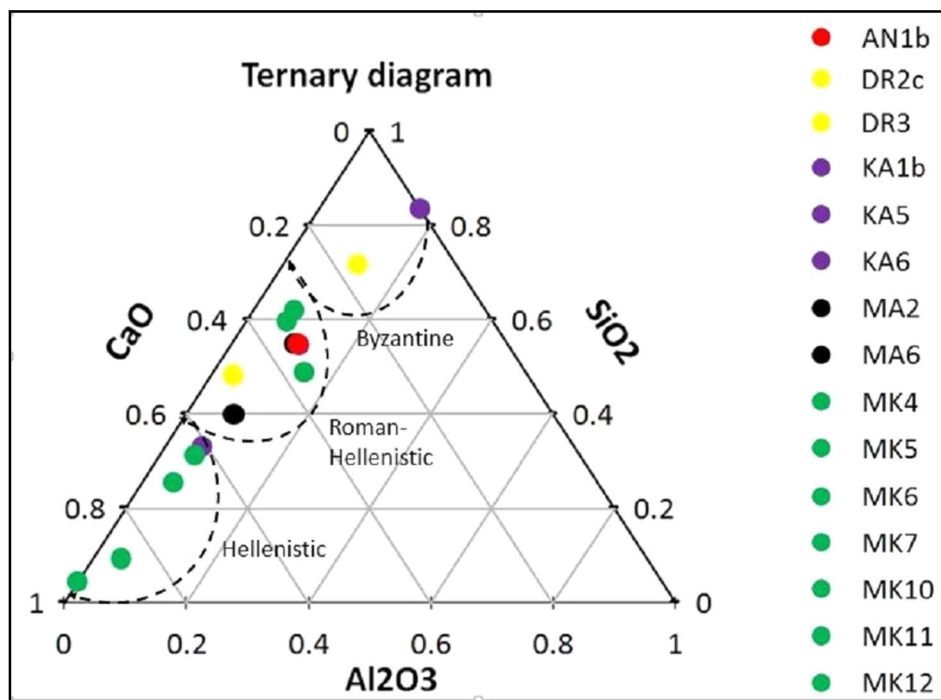


**Figure 10.** CaO-Al<sub>2</sub>O<sub>3</sub>-SiO<sub>2</sub>% ternary plot of Energy Dispersive X-ray (EDX) analyses of data collected from mortar samples: Hellenistic mortars (MK4-12), Roman mortars (A1b, DR2c, DR3), Byzantine mortars (KA1β, K5, K3A).

### 3.2. Stable Isotope Analysis

The  $\delta^{13}\text{C}$  and  $\delta^{18}\text{O}$  of calcite matrix of the Byzantine, Late Roman and Hellenistic mortar indicate a wide range of isotopic values ranging between  $-17.1\text{‰}$  to  $1.2\text{‰}$  and  $-25.9\text{‰}$  to  $-2.0\text{‰}$ , respectively (Table 2). Additional samples of local marine limestone of Cretaceous age were obtained. These samples are located in the vicinity of the historical buildings and they were used as ancient raw materials for burning. The limestones comprise a range of  $\delta^{13}\text{C}$  values between 0 and  $3\text{‰}$  and of  $\delta^{18}\text{O}$  between  $-5\text{‰}$  and  $-2\text{‰}$  [19] indicating that the isotopic compositions of the calcite matrix from historical mortar are in general lighter, compared to those of local limestone. These light isotopic values are attributed to the absorption of carbon dioxide from the atmosphere within the setting of lime mortar ( $^{13}\text{C}_{\text{CO}_2} = -6$ ).

22 drill-core samples (presented in Table 2 and they represent samples with increasing isotopic values from the exterior to the interior layer) were examined in order to create an ideal Hellenistic and Byzantine mortar layer and to provide weathering gradients using isotopic analysis. The isotopic values of lime-pozzolan and lime mortar are shown in (Figure 11). In Table 3 we present the results of cross-section analysis. The isotopic values of these samples comprise a range of  $\delta^{13}\text{C}$  and  $\delta^{18}\text{O}$  values from  $-13.6\text{‰}$  to  $3.6\text{‰}$  and from  $-12.6\text{‰}$  to  $0.4\text{‰}$ , respectively. Most of these samples indicate that calcite matrix is isotopically heavier inside the mortar layer, compared to those of the exterior layer, probably due to the reaction of atmospheric  $\text{CO}_2$  with the lime mortar. A positive correlation of  $\delta^{13}\text{C}$  vs.  $\delta^{18}\text{O}$  of calcite is observed that is expressed by the regression lines  $\delta^{18}\text{O}_{\text{calcite matrix}} = 0.61 \times \delta^{13}\text{C}_{\text{calcite matrix}} - 1.8$  (lime mortars line in Figure 11) and  $\delta^{18}\text{O}_{\text{calcite matrix}} = 0.63 \times \delta^{13}\text{C}_{\text{calcite matrix}} - 2$  (hydraulic mortars line in Figure 11) for Hellenistic and Byzantine mortar, respectively. The slope of these equations is close to that is expressed by the experimentally obtained equation from Kosednar Legenstein et al., [20].

**Table 2.** List of analyzed samples and their isotopic value.

SampleID	Observation	$\delta^{13}\text{C}$ (‰ VPDB)	$\delta^{18}\text{O}$ (‰ VPDB)	Location
AN1a-1	Ext.Joint	-12.9	-16.1	Anaktoroupoli, Kavala
AN2a-1	Ext.Joint	-10.0	-9.2	Anaktoroupoli, Kavala
AN2a-2	Ext.Joint	-5.8	-5.5	Anaktoroupoli, Kavala
AN3a-1	Ext.Joint	-0.4	-2.4	Anaktoroupoli, Kavala
AN1b-1	Ext.Joint	-15.7	-12.5	Anaktoroupoli, Kavala
AN9-1	Ext.Joint	-8.7	-6	Anaktoroupoli, Kavala
Anp-1	Ext.Joint	-9.9	-4.9	Anaktoroupoli, Kavala
DRa-1	Ext.Joint	-10.0	-9.2	Drama
DRa-2	Ext.Joint	-17.1	-25.9	Drama
DR1b-1	Ext.Joint	-8	-13.4	Drama
DR2a-1	Ext.Joint	-8.9	-13.2	Drama
DR2c-1	Ext.Joint	-13.7	-16.1	Drama
DR5a-1	Ext.Joint	-12.9	-16.1	Drama
DR5b-1	Ext.Joint	-15.6	-10.5	Drama
DR2g-1	Ext.Joint	-6.6	-7.5	Drama
MA1-3	Ext.Joint	-10.9	-17.6	Marmarion Tower, Kavala
MA3-1	Ext.Joint	-8.3	-14.4	Marmarion Tower, Kavala
MA5-1	Ext.Joint	-5	-10.7	Marmarion Tower, Kavala
MA5-2	Int.joint	-8.3	-10	Marmarion Tower, Kavala
MK1-1	Rend.Ext.	-12.3	-6.3	Makrygialos
MK1-2	Rend.Int	-13.8	-9.1	Makrygialos
MK1-3	Rend.Int	-14.4	-9.5	Makrygialos
MK2-1	Rend.Ext.	-6.2	-4.6	Makrygialos
MK2-3	Rend.Int	-9.4	-7.3	Makrygialos
MK3-1	Rend.Ext.	-10.4	-8.7	Makrygialos
MK4-1	Rend.Ext.	-9.4	-6.4	Makrygialos
MK4-2	Rend.Int	-10.9	-9.1	Makrygialos
MK5-1	Rend.Ext.	-9.3	-5.7	Makrygialos
MK5-2	Rend.Int	-9.6	-7.1	Makrygialos
MK6-1	Rend.Ext.	0.1	-2.0	Makrygialos
MK6-2	Rend.Int	-9.9	-4.9	Makrygialos
MK7-1	Rend.Ext.	-5.0	-6.2	Makrygialos
MK7-2	Rend.Int	-8.7	-6.0	Makrygialos
MK8-1	Rend.Ext.	1.2	-2.1	Makrygialos
M8-2	Rend.Int	-3.0	-3.3	Makrygialos
MK9-1	Rend.Ext.	-0.4	-2.4	Makrygialos
MK9-2	Rend.Int	-10.6	-6.7	Makrygialos
MK10-1	Rend.Ext.	-5.8	-5.5	Makrygialos
MK10-2	Rend.Int	-3.0	-3.4	Makrygialos

Notes (Description of the type of mortar layer): Ext.joint = external joint; Int.joint = internal joint; Rend.Ext = rendering external; Rend.Int = rendering internal.

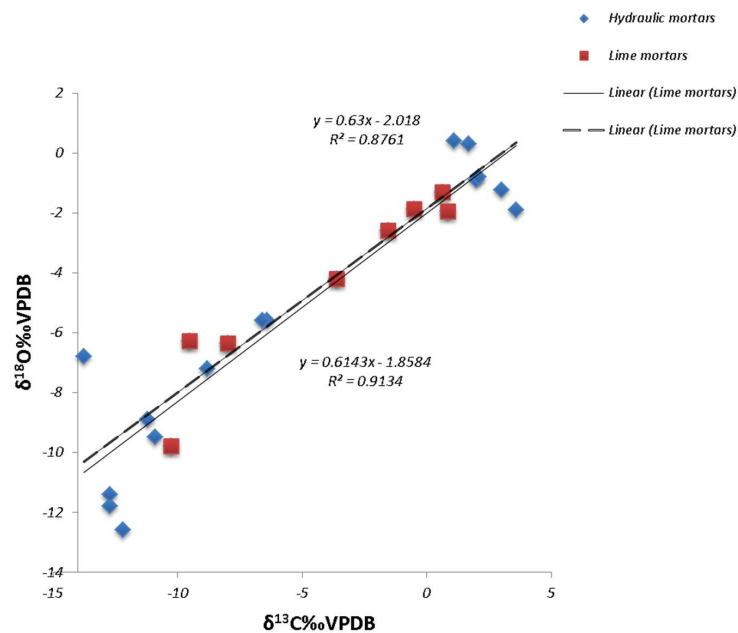


**Figure 11.**  $\delta^{13}\text{C}$  vs.  $\delta^{18}\text{O}$  for all the samples. Regression lines for hydraulic and lime mortars.

**Table 3.** List of cross-section analysis.

Sample ID	Depth (cm)	$\delta^{13}\text{C}$ (‰ VPDB)	$\delta^{18}\text{O}$ (‰ VPDB)
Hydraulic. (lime-pozzolan) mortars. (Kavala. Drama)	−6	3.6	−1.9
	−6	3	−1.3
	−6	2	−0.9
	−6	1.7	0.3
	−6	1.1	0.4
	−3	−6.4	−5.6
	−3	−6.6	−5.6
	−3	−8.8	−7.2
	+0	−10.9	−9.5
	+0	−12.2	−12.6
	+0	−11.2	−8.9
	+0	−12.7	−11.8
	+0	−12.7	−11.4
	+0	−13.6	−6.8
	Lime mortars (Hellenistic mortars. Makrygialos)	−6	0.7
−6		0.9	−2
−6		−0.5	−1.9
−3		−1.6	−2.6
−3		−3.6	−4.2
+0		−8	−6.4
+0		−9.5	−6.3
+0		−10.3	−9.8

These lines comprise ideal mortar layers representing continuous calcite formation with continuous enrichment of  $^{18}\text{O}$  versus  $^{16}\text{O}$  and  $^{13}\text{C}$  vs.  $^{12}\text{C}$  in the  $\text{CO}_2$  gas phase and the precipitated calcite. It appears that the quantity percentage and the quality of the charge do not influence significantly the  $^{13}\text{C}$  of carbonate formed. The other data from mortars lie close or below this line indicating different setting environments and secondary effects. Also, in most Hellenistic samples it is noted that at interior levels the calcite is depleted in  $^{13}\text{C}$ , compared to the middle layer. This depletion in  $^{13}\text{C}$  can be explained by the heterogeneity of lime mortar, because this material is not chemically homogenous [36]. Also, higher  $\delta^{18}\text{O}$  values are present in the near surface layer. The enrichment in  $^{18}\text{O}$  in the near-surface layers is due to the contribution of water even if only 1/3 of the oxygen in the solid carbonate came from the water. Consequently, despite the contribution of water is minor, it causes this “surface effect” or oxygen enrichment because of important evaporation of water especially near the surface of the mortar (see Section 4.2 for further analysis).

## 4. Discussion

### 4.1. Technological Variations and Degradation Mechanisms

In comparing the technology of Hellenistic mortars from Makrygialos Greece with the later mortars (Roman and Byzantine) the first aspect to emphasize is that the lime-based mortars used in funerary monuments in Makrygialos were replaced with advanced lime-pozzolan mortars in Roman and Byzantine constructions. The content of lime in Hellenistic mortars approaches the 96%, whereas the content of lime in Roman and Byzantine mortars is between 30% and 90%. Furthermore, the aggregates in Hellenistic mortars are composed of quartz, plagioclase and potassium feldspar, whereas the aggregates of later mortars are composed of quartz, plagioclase, potassium feldspar, microcline, crushed ceramic and lithoclasts. The ternary plot (Figure 10) depicts the differentiations in mortar composition, since mortar samples obtained from Makrygialos are concentrated in the corner that expresses the maximum content of (CaO), moreover Roman and Byzantine mortars are concentrated in the corner with maximum content of ( $\text{SiO}_2$ ). Roman and Byzantine mortars demonstrate coherence and strength since pozzolan is added to the binding material. The addition of pozzolanic materials enhances the power of the mortars and reduces the pore structure [37–39]. The addition of crushed ceramics as aggregates can trigger reactions on the fragment-lime interface [17,40] and the penetration of lime into the smaller pores of the ceramic

fragments increases the apparent density which in turn increases the mortar strength, turning them suitable to support heavy historic constructions.

#### 4.2. Evaluation of Setting Environments and Processes

The stable isotope ( $^{13}\text{C}$  and  $^{18}\text{O}$ ) analysis is related to the conditions of formation and the origin of the carbonates and therefore it is a useful tool for providing extra parameters, associated with the diagnostic of the mechanisms and processes that cause material degradation. The carbon and oxygen isotopes in mortar were analyzed in order to evidence the carbonate origin and to identify the potential sources of mortar decay such as salts attack, signs of sulfation and dissolution/recrystallization processes. All the mechanisms and processes related to mortar degradation are depicted in Figure 12. Figure 12 shows the various sources of  $\text{CO}_2$  and  $\text{H}_2\text{O}$  (lines) and mechanisms (areas). line 1 is the equation  $\delta^{18}\text{O}_{\text{calcite}} = 0.63 \times \delta^{13}\text{C}_{\text{calcite}} - 2$  and line 1a is the deviation from line 1 due to relicts of local limestone used for burning or contamination by limestone aggregates; line 2a the primary source of water used for setting of the lime mortar is originating from heavy source—evaporation effect. Point CM indicates that precipitated calcite is formed directly by the absorption of atmospheric  $\text{CO}_2$  in strong alkaline aqueous environment; its values change to more enriched isotopic composition due to continuous enrichment of  $\delta^{13}\text{C}$  of  $\text{CO}_2$  during calcite precipitation; area A: defined by 1 and 1a lines, precipitated calcite formed from atmospheric  $\text{CO}_2$  and contaminated by residual natural limestone; area B indicates that precipitated calcite is formed from atmospheric  $\text{CO}_2$  and heavy, evaporated water. Enrichment of C and O isotopes indicates recrystallization of calcite with water of meteoric origin and atmospheric  $\text{CO}_2$ ; area B2 these samples demonstrate enrichment in  $^{18}\text{O}$  of calcite due to equilibrium to silicate minerals.; area C precipitated calcite formed from atmospheric  $\text{CO}_2$  and isotopically light local meteoric water or isotopically light recondensed primary waters.; area C1, depletion of C and O isotopes, indicates also human influence (surface treatment) and biological growth; Figure 13 presents a simplification of Figure 12. The blue arrow indicates the enrichment of  $^{18}\text{O}$  of calcite due to the equilibrium with the silica mineral, whereas the red arrow denotes the enrichment of  $^{18}\text{O}$  of precipitated calcite formed from atmospheric  $\text{CO}_2$  and heavy evaporated water.

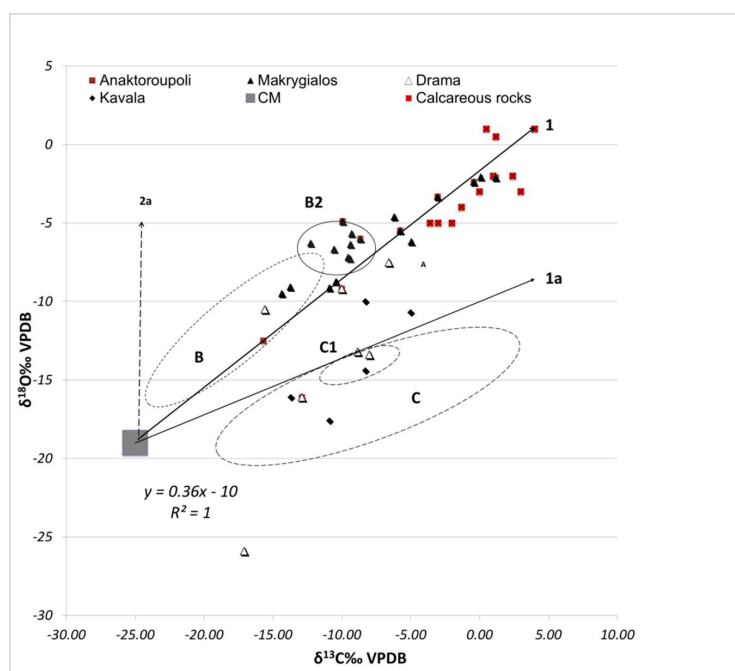


**Figure 12.** Scattered diagram that summarizes the various sources of  $\text{CO}_2$  and  $\text{H}_2\text{O}$  (lines) and mechanisms (areas).

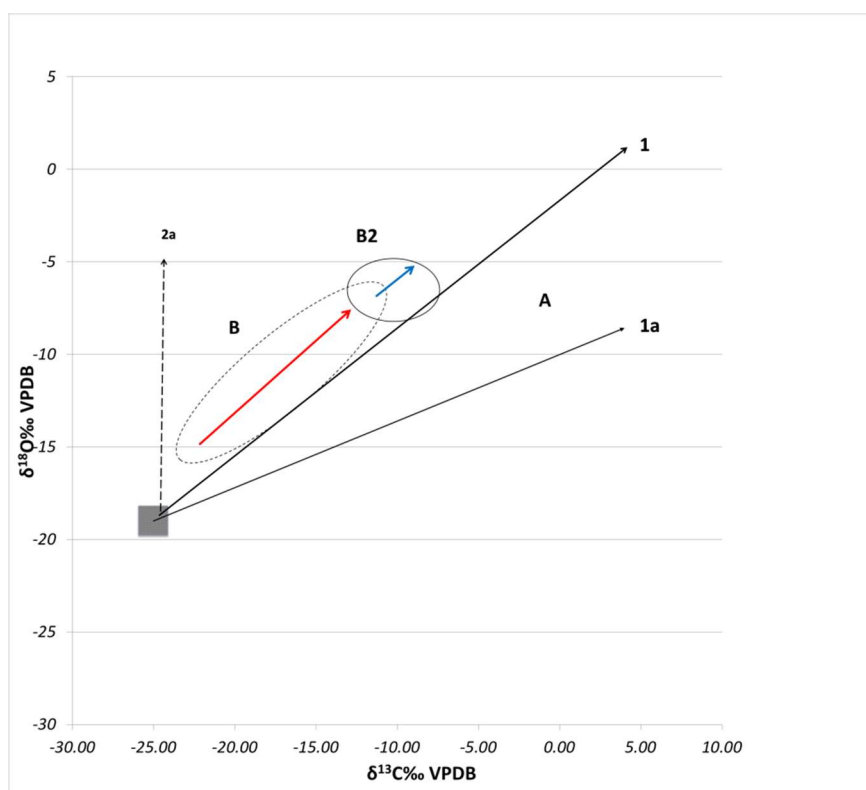


**Figure 13.** The blue arrow indicates the enrichment of  $^{18}\text{O}$  of calcite due to the equilibrium with the silica mineral, whereas the red arrow denotes the enrichment of  $^{18}\text{O}$  of precipitated calcite formed from atmospheric  $\text{CO}_2$  and heavy evaporated water.

The isotopic composition of calcite from mortar represent non-isotopic equilibrium [19,20,41–45] and depends mainly on the isotopic composition of atmospheric  $\text{CO}_2$  and water and on the degree to which the isotopic equilibrium is reached and therefore the factor of fractionation of  $\delta^{13}\text{C}_{\text{CaCO}_3} - \delta^{13}\text{C}_{\text{CO}_2} - \delta^{18}\text{O}_{\text{CO}_2}$  and  $\delta^{18}\text{O}_{\text{H}_2\text{O}}$ . In order to define the isotopic values for a pure calcite precipitated in alkaline environment using local meteoric water and atmospheric  $\text{CO}_2$ , the isotopic values of local water in each sampling area are analyzed. The isotopic values of rain and spring water of the area where the ancient monuments are located are:  $-7.2\text{‰}^{18}\text{O}$  and  $-45\text{‰}^2\text{H}$  for samples from Makrygialos,  $-6.5\text{‰}^{18}\text{O}$  and  $-38\text{‰}^2\text{H}$  for samples from Kavala and  $-8\text{‰}^{18}\text{O}$  and  $-65\text{‰}^2\text{H}$  for samples from Drama [46]. Moreover, evaporation of water during the setting of the mortar gives isotopically heavier residual water. In contrary condensation effect gives isotopically lighter residual water. The origin of atmospheric  $\text{CO}_2$  for calcite formation is another important factor. It can be presumed that the isotopes of C and O of  $\text{CO}_2$  (of atmospheric origin) were stable for the last two decades. However, air pollution is not a new problem. In ancient Rome glassworkers moved outside the city centre because of environmental nuisance [47].  $\text{CO}_2$  of biogenic origin, (combustion of coal, fuel or soil  $\text{CO}_2$ ) presents very low  $\delta^{13}\text{C}$  [19].

Therefore, considering the isotope fractionation of C between the  $\text{CO}_2$  (gas) and the precipitated calcite in alkaline environment the  $\delta^{13}\text{C}_{\text{calcite-CO}_2} = \delta^{13}\text{C}_{\text{calcite}} - \delta^{13}\text{C}_{\text{CO}_2} = -18\text{‰}$  [20] and considering that the values for  $\delta^{13}\text{C}_{\text{CO}_2}$  range between  $-7\text{‰}$  and  $-9\text{‰}$ , it is possible to calculate the  $\delta^{13}\text{C}_{\text{calcite}}$  that is between  $-25\text{‰}$  and  $-27\text{‰}$ . Regarding the  $\delta^{18}\text{O}$ , both the water and the  $\text{CO}_2$  oxygen contribute to the precipitated carbonate. Usdowski and Hoefs [48] and O'Neil and Barnes [41] have demonstrated that in alkaline environments, 2/3 of the oxygen in precipitated carbonate comes directly from  $\text{CO}_2$  and 1/3 of the  $\delta^{18}\text{O}$  comes from  $\text{OH}^-$ . Considering the mean temperature in Makrygialos and East Macedonia and considering also the isotope fractionation between  $\text{H}_2\text{O}$  and  $\text{OH}^-$  ( $\alpha_{\text{H}_2\text{O} - \text{OH}^-} = 1.042 - 1$ ,  $T = 20^\circ\text{C}$ ), the value of  $\delta^{18}\text{O}_{\text{OH}^-}$  [ $\delta^{18}\text{O}_{\text{OH}^-} = \delta^{18}\text{O}_{\text{H}_2\text{O}} - (\alpha_{\text{H}_2\text{O} - \text{OH}^-} - 1) \times 1000$ ] is calculated

between  $-78\text{‰}$  and  $-80\text{‰}$ . Taking into consideration that the  $\delta^{18}\text{O}$  of  $\text{CO}_2$  is  $10\text{‰}$ , (VPDB), the  $\delta^{18}\text{O}_{\text{calcite}}$  is calculated ( $\delta^{18}\text{O}_{\text{calcite}} = 1/3 \times \delta^{18}\text{O}_{\text{OH}^-} + 2/3 \times \delta^{18}\text{O}_{\text{CO}_2}$ ) between  $-19\text{‰}$  and  $-20\text{‰}$ . Therefore, such C and O isotopes values  $\delta^{13}\text{C}_{\text{calcite}} = -25\text{‰}$  to  $-27\text{‰}$  and  $\delta^{18}\text{O}_{\text{calcite}} = -19\text{‰}$  to  $-20\text{‰}$  (area CM in Figure 12) are typical for the precipitation of calcite by atmospheric  $\text{CO}_2$  absorption using the local isotopic composition of Drama, Kavala and Makrygialos water and atmospheric  $\text{CO}_2$ .

However, the carbon and oxygen isotopic value could change due to continuous enrichment of  $^{13}\text{C}$  relative to  $^{12}\text{C}$  and of  $^{18}\text{O}$  relative to  $^{16}\text{O}$  for the  $\text{CO}_2$  gas phase and the precipitated calcite due to kinetic isotope fractionation, during calcite formation. This positive correlation of  $\delta^{13}\text{C}/\delta^{18}\text{O}$  of the formed calcite in our historical mortar made possible to determine the ideal layer from Hellenistic period and is represented by the equation  $\delta^{18}\text{O}_{\text{calcite}} = 0.63 \times \delta^{13}\text{C}_{\text{calcite}} - 2$  (line 1 in Figure 12). Moreover, the  $\delta^{13}\text{C}$  of mortar is also affected by the mortar mixing composition (the parts of mixing between lime, water, sand and old calcite or aggregate). If the lime is pure  $\text{CaO}$  (100%), then the carbonate formed, still has not attained a steady isotopic composition and presents  $\delta^{13}\text{C}$  and  $\delta^{18}\text{O}$   $-22\text{‰}$  and  $-20\text{‰}$ , respectively. These isotopic values change as the amount of charge increases (because the  $\delta^{13}\text{C}$  of old calcite is approximately  $0\text{‰}$ ) and the  $\delta^{13}\text{C}$  of carbonate formed depends on the mixing percentage of  $\text{CaO}$  and sand-old calcite. The percentage of  $\text{CaO}$  in Hellenistic samples is between 50% and 95% (Table 1). So, for a mix of equal quantities of  $\text{CaO}$  (50%) and sand-old calcite (50%), the  $\delta^{13}\text{C}$  is  $-9.5\text{‰}$  while, when the percentage of  $\text{CaO}$  is higher due to the addition of small quantities of sand and old calcite, the  $\delta^{13}\text{C}$  of carbonate formed is more negative. Additionally, local marine limestone (Cretaceous carbonate) in the vicinity of the historical buildings, which was the main source of ancient raw material for burning, has  $\delta^{13}\text{C}$  between 0 and  $3\text{‰}$  and  $\delta^{18}\text{O}$  between  $-5\text{‰}$  and  $-2\text{‰}$  (Figure 12). Therefore, it is expected that the old mortars, which are a mixture of lime, water, sand and an aggregate like reworked brick and marble, would have  $\delta^{13}\text{C} > -25\text{‰}$  or heavier depending on the percentage of participation of old calcite. Taking into account the percentage of  $\text{CaO}$  in Hellenistic samples the  $\delta^{13}\text{C}$  of carbonate formed will be between  $-25\text{‰}$  and  $-9.5\text{‰}$  depending on the participation of old calcite aggregates. In fact the Hellenistic samples show a positive correlation between  $\delta^{13}\text{C}$  and charge indicating that the shift, to more positive values can be caused by residual limestone. Consequently, the percentage of limestone used for burning or the  $\text{CO}_2$  absorption is competitive against the final value of  $^{13}\text{C}$  (lines 1 and 1a, Figure 12).

Mineralogical, morphological and chemical analysis indicated that the hydraulic mortars are attacked by salts while the lime-based mortars are decomposed because of the leaching action that causes material dissolution/recrystallization processes. This is depicted in Figure 12, since samples from Makrygialos are concentrated in area B2;  $\delta^{18}\text{O}$  values of these samples demonstrate continues enrichment and recrystallization tendency in O, which is related to the changes in isotopic composition because of recrystallization/dissolution mechanisms. Additionally, most of the data lie close or between on these lines indicating that the isotopic values reflect increasing  $\delta^{13}\text{C}$  values of  $\text{CO}_2$  with calcite formation along the mortar layer and the contamination by impurities of limestone relict.

However, a certain number of data (samples from Marmarion MA1-3, MA5-1 and Drama DR2g-1, DR2a-1, samples from Makrygialos and calcareous rocks) lie on or beyond of this area (area A defined by 1 and 1a lines) indicating different setting environment and secondary effects. A moderate oxygen isotopic shift is observed for samples from Makrygialos indicating that the variability of ancient water influenced the isotopic composition of calcite. Also, the oxygen values of the precipitated calcite shift to heavier values because of the evaporation of water (line 2a, area B) during the setting of mortar. Moreover, the mineralogical, morphological and chemical analysis showed that samples from Anaktoroupoli (Anp-1), Drama (DR5b-1) and some from Makrygialos (MK10-2, MK5) demonstrate intensive fragmentation, cracks and extensive deposition of salts that indicates later calcite alteration with actual meteoric water. There seems to be a moderate enrichment of  $\delta^{18}\text{O}$  at the surface indicating influence from rain evaporated water and from capillary suction of water. In this case the capillary transport of water was followed by evaporation when equilibrium between capillary addition of water and evaporation is reached and by salt precipitation. Thus, the major processes are dissolution of

calcite and probably precipitation of other minerals (Area B2). Most of the samples lying in area B2 come from Makrygialos. SEM analysis for these samples elucidated evidence of recrystallization and material dissolution. The rest of the samples (mainly from Makrygialos) present positive oxygen isotopic shift and also significant change of the initial carbon. These isotopic values may be caused by the recrystallization of calcite with porewater and CO<sub>2</sub> of various sources. Secondary solutions for recrystallization will be rain water and then the δ<sup>18</sup>O of calcite matrix should shift to heavier values, in our case around 0‰ similar to isotopic values of limestone. Values around 0‰, also for oxygen and carbon are attributed in the fine calcite particles (according to mineralogical, morphological and chemical analysis) in the matrix due to limestone relicts that are derived from insufficient burning. A group of data lie beyond area A indicating that precipitated calcite is formed from atmospheric CO<sub>2</sub> and isotopically light local meteoric water or isotopically light re-condensed primary water (area C); also line 2a depicts the depletion of both isotopes indicating recrystallization of calcite with light water and CO<sub>2</sub> of mixed origin (atmospheric and soil origin).

## 5. Conclusions

This work indicated that the use of isotope methods in addition to the existing “toolbox” (mineralogical, morphological, chemical analysis) of pre-restoration research methods will help to better direct safeguarding and conservation measures. The diagnostic contribution of stable isotope study traces the various sources and possible secondary processes that are responsible for the mortar degradation. Stable isotope analysis applied in combination with mineralogical, microscopic and elemental analysis provided information on the different types of mortar degradation. Mortar’s weathering was attributed to a combination of environmental threats such as salts attack and leaching action. Stable isotope analysis (<sup>13</sup>C and <sup>18</sup>O) provided information relative to the origin of CO<sub>2</sub> and water during calcite formation making possible to distinguish different mortar technologies and degradation gradients. Compositional and morphological analyses were achieved using energy dispersive X-ray analysis in the scanning electron microscope while the mineralogical phases were detected using petrographic (polarized optical microscopy) analysis. The results of micro-morphological and petrographic examination elucidated the technological continuity and degradation of historic mortars. Hellenistic mortars are composed of lime enhanced with quartz aggregates. Roman and Byzantine mortars are composed of hydraulic lime, pozzolan and a various aggregates such as quartz, feldspar, ceramic and lithoclasts. The main degradation mechanisms are calcite recrystallization, loose of adhesion bonds in the binding material and salts crystallization. Mortar’s weathering was also attributed to a combination of environmental threats such as salts attack and leaching action. Stable isotopes of δ<sup>18</sup>O and δ<sup>13</sup>C showed that in general there are extended dissolution/precipitation processes that take place on the surface layers ending in the inner structure of funerary monuments. Finally, this study indicated that stable isotope analysis is an excellent tool to fingerprint the origin of carbonate and therefore indicate the variations in mortar’s technology, the environmental setting conditions of mortar, origin of CO<sub>2</sub> and water during calcite formation and to determine the weathering depth and the potential secondary degradation mechanisms.

**Author Contributions:** Conceptualization, D.E; Methodology, D.E, K.D., C.V. and D.G. Writing–Original Draft Preparation, D.E., K.D.; Writing–Editing, D.G.; Project Administration, D.E.; Funding Acquisition, D.E.

**Funding:** This research received no external funding.

**Acknowledgments:** We would like to sincerely thank Bessios at the KZ’ Ephoreia of Classical and Prehistoric antiquities for kindly providing access for sampling at Hellenistic funerary monuments. Also, Dadaki and Ioannis Iliadis at the 12th Ephoreia of Byzantine antiquities are kindly thanked for providing Byzantine and Roman mortar samples. Finally, many thanks go to Vasilios Melfos for performing petrographic analysis in mortar samples at the Department of Mineralogy, Petrology and Economic Geology in Aristotle University of Thessaloniki.

**Conflicts of Interest:** The authors declare no conflict of interest.

## References

1. Sabbioni, C.; Zappia, G.; Riontino, C.; Blanco-Varela, M.T.; Aguilera, J.; Puertas, F.; Van Balen, K.; Toumbakari, E.E. Atmospheric deterioration of ancient and modern hydraulic mortars. *Atmos. Environ.* **2001**, *35*, 539–548. [[CrossRef](#)]
2. van Balen, K.; Toumbakari, E.E.; Blanco-Varela, M.T.; Aguilera, J.; Puertas, F.; Palomo, A. Environmental deterioration of ancient and modern hydraulic mortars. *WIT Trans. Built Environ.* **1970**, *42*, 10.
3. Yates, T. *The Effects of Air Pollution on the Built Environment*. *Air Pollution Reviews*; Brimblecombe, P., Ed.; Imperial College Press: London, UK, 2003; pp. 107–132.
4. Zappia, G.; Sabbioni, C.; Pauri, M.; Gobbi, G. Mortar damage due to airborne sulfur compounds. *Mater. Struct.* **1994**, *27*, 469–473. [[CrossRef](#)]
5. Stefanidou, M.; Papayianni, I. Salt accumulation in historic and repair mortars. In Proceedings of the Heritage, Weathering and Conservation Conference, Consejo Superior de Investigaciones Científicas, Madrid, Spain, 21–24 June 2006; Taylor & Francis: London, UK, 2006; pp. 269–272.
6. Stefanidou, M. A contribution to salt crystallization into the structure of traditional repair mortars through capillarity. In Proceedings of the 11th euroseminar on microscopy applied to building materials, Porto, Portugal, 5–9 June 2007.
7. Theoulakis, P.; Moropoulou, A. Microstructural and mechanical parameters determining the susceptibility of porous building stones to salt decay. *Constr. Build. Mater.* **1997**, *11*, 65–71. [[CrossRef](#)]
8. Rossi-Manaresi, R.; Tucci, A. Pore structure and the disruptive or cementing effect of salt crystallization in various types of stone. *Stud. Conserv.* **1991**, *36*, 56–58.
9. Scherer, G.W. Stress from crystallization of salt. *Cem. Concr. Res.* **2004**, *34*, 1613–1624. [[CrossRef](#)]
10. Papayianni, I.; Stefanidou, M.; Pachta, V.; Konopisi, S. Content and topography of salts in historic mortars. In Proceedings of the 3rd Historic mortars conference, Glasgow, Scotland, 11–14 September 2013.
11. Gomides, M.d.J.; Molin, D.C.C.D.; Rêgo, J.H.d.S. Effect of the incorporation of aggregates with high sulfide content on the mechanical and microstructural properties of concrete with slag cement. *Matéria (Rio de Janeiro)* **2017**, *22*. [[CrossRef](#)]
12. Chinchón, J.; Ayora, C.; Aguado, A.; Guirado, F. Influence of weathering of iron sulfides contained in aggregates on concrete durability. *Cem. Concr. Res.* **1995**, *25*, 1264–1272. [[CrossRef](#)]
13. Clark, I.; Fritz, P. *Environmental Isotopes in Hydrogeology*; Lewis Publishers: Boca Raton, FL, USA, 1997.
14. Craig, H. Isotopic variations in meteoric waters. *Science* **1961**, *133*, 1702–1703. [[CrossRef](#)] [[PubMed](#)]
15. Maravelaki-Kalaitzaki, P.; Bakolas, A.; Moropoulou, A. Physico-chemical study of Cretan ancient mortars. *Cement and Concrete Research* **2003**, *33*, 651–661. [[CrossRef](#)]
16. Moropoulou, A.; Bakolas, A.; Bisbikou, K. Investigation of the technology of historic mortars. *J. Cult. Her.* **2000**, *1*, 45–58. [[CrossRef](#)]
17. Moropoulou, A.; Bakolas, A.; Bisbikou, K. Characterization of ancient, byzantine and later historic mortars by thermal and X-ray diffraction techniques. *Thermochim. Act.* **1995**, *269*, 779–795. [[CrossRef](#)]
18. Bakolas, A.; Biscontin, G.; Moropoulou, A.; Zendri, E. Characterization of the lumps in the mortars of historic masonry. *Thermochim. Acta* **1995**, *269*, 809–816. [[CrossRef](#)]
19. Dotsika, E.; Psomiadis, D.; Raco, B.; Poutoukis, D.; Gamaletsos, P. Isotopic analysis for degradation diagnosis of calcite matrix in mortar and plaster. *Anal. Bioanal. Chem.* **2009**, *395*, 2227–2234. [[CrossRef](#)] [[PubMed](#)]
20. Kosednar-Legenstein, B.; Dietzel, M.; Leis, A.; Stingl, K. Stable carbon and oxygen isotope investigation in historical lime mortar and plaster—Results from field and experimental study. *Appl. Geochem.* **2008**, *23*, 2425–2437. [[CrossRef](#)]
21. Larbi, J. Microscopy applied to the diagnosis of the deterioration of brick masonry. *Constr. Build. Mater.* **2004**, *18*, 299–307. [[CrossRef](#)]
22. Hughes, J.J.; Cuthbert, S.J. The petrography and microstructure of medieval lime mortars from the west of Scotland: Implications for the formulation of repair and replacement mortars. *Mater. Struct.* **2000**, *33*, 594–600. [[CrossRef](#)]
23. Deer, W.A.; Howie, R.A.; Zussman, J. *An Introduction to the Rock Forming Minerals*, 2nd ed.; Longman Scientific & Technical: London, UK, 1992; p. 696.
24. Tucker, M.E. *Sedimentary Petrology*, 2nd ed.; Blackwell Scientific Publications: Hoboken, NJ, USA, 1991.

25. Adams, A.E.; MacKenzie, W.S.; Guildford, C. *Atlas of Sedimentary Rocks Under the Microscope*; Routledge: Abington, UK, 2017.
26. Whitbread, I.K. The characterisation of argillaceous inclusions in ceramic thin sections. *Archaeometry* **1986**, *28*, 79–88. [[CrossRef](#)]
27. Freestone, I.C. Ceramic Petrography. *Am. J. Archaeol.* **1995**, *99*, 111–115.
28. Coplen, T.B.; Kendall, C.; Hopple, J. Comparison of stable isotope reference samples. *Nature* **1983**, *302*, 236–238. [[CrossRef](#)]
29. Coplen, T.B. Reporting of stable hydrogen, carbon and oxygen isotopic abundances (technical report). *Int. Union Pure Appl. Chem.* **1994**, *66*, 273–276. [[CrossRef](#)]
30. Coplen, T.B. Discontinuance of Smow and PDB. *Nature* **1995**, *375*, 285. [[CrossRef](#)]
31. Chabas, A.; Jeannette, D. Weathering of marbles and granites in marine environment: petrophysical properties and special role of atmospheric salts. *Environ. Geol.* **2001**, *40*, 359–368. [[CrossRef](#)]
32. Liu, P. Damage to concrete structures in a marine environment. *Mater. Struct.* **1991**, *24*, 302–307. [[CrossRef](#)]
33. Tsouris, E.M.A. Byzantine fortifications in Evros. *Byzantina* **2006**, *26*, 153–209.
34. Dadaki, S. (Greek Ministry of Culture, Athens, Greece). Historical overview of the antiquities of 12th EBA, 12th Ephoreia of Byzantine antiquities, Archaeological report. Unpublished work, 2010.
35. Mpesios, M. *Pieridon Stephanos: Pydna, Methone Kai Hoi Archaioetes Tes Voreias Pierias*; Anthropon Physeos Erga: Katerine, Greece, 2010.
36. van Strydonck, M.J.; Dupas, M.; Keppens, E. Isotopic fractionation of oxygen and carbon in lime mortar under natural environmental-conditions. *Radiocarbon* **1989**, *31*, 610–618. [[CrossRef](#)]
37. Papayianni, I.; Stefanidou, M. Strength–porosity relationships in lime–pozzolan mortars. *Constr. Build. Mater.* **2006**, *20*, 700–705. [[CrossRef](#)]
38. Walker, R.; Pavía, S. Behaviour and Properties of Lime-Pozzolan Pastes. In Proceedings of the 8th International Masonry Conference 2010, Dresden, Germany, 4–7 July 2010; Jäger, W., Haseltine, B., Fried, A., Eds.; International Masonry Society: Shermanbury, UK, 2010; pp. 353–362.
39. Walker, R.; Pavía, S. Physical properties and reactivity of pozzolans, and their influence on the properties of lime-pozzolan pastes. *Mater. Struct.* **2011**, *44*, 1139–1150. [[CrossRef](#)]
40. Matias, G.; Faria, P.; Torres, I. Lime mortars with heat treated clays and ceramic waste: a review. *Constr. Build. Mater.* **2014**, *73*, 125–136. [[CrossRef](#)]
41. O’Neil, J.R.; Barnes, I.  $^{13}\text{C}$  and  $^{18}\text{O}$  compositions in some fresh-water carbonates associated with ultramafic rocks and serpentinites: Western United States. *Geochim. Cosmochim. Acta* **1971**, *35*, 687–697. [[CrossRef](#)]
42. Pachiaudi, C.; Marechal, J.; van Strydonck, M.; Dupas, M.; Dauchot-Dehon, M. Isotopic fractionation of carbon during  $\text{CO}_2$  absorption by mortar. *Radiocarbon* **1986**, *28*, 691–697. [[CrossRef](#)]
43. Rafai, N.; Letolle, R.; Blanc, P.; Gegout, P.; Revertegat, E. Carbonation–decarbonation of concretes studied by the way of carbon and oxygen stable isotopes. *Cem. Concr. Res.* **1992**, *22*, 882–890. [[CrossRef](#)]
44. Dietzel, M.; Usdowski, E.; Hoefs, J. Chemical and  $^{13}\text{C}/^{12}\text{C}$  and  $^{18}\text{O}/^{16}\text{O}$ -isotope evolution of alkaline drainage waters and the precipitation of calcite. *Appl. Geochem.* **1992**, *7*, 177–184. [[CrossRef](#)]
45. Clark, I.D.; Fontes, J.C.; Fritz, P. Stable isotope disequilibria in travertine from high pH waters: Laboratory investigations and field observations from Oman. *Geochim. Cosmochim. Acta* **1992**, *56*, 2041–2050. [[CrossRef](#)]
46. Dotsika, E.; Lykoudis, S.; Poutoukis, D. Spatial distribution of the isotopic composition of precipitation and spring water in Greece. *Glob. Planet. Chang.* **2010**, *71*, 141–149. [[CrossRef](#)]
47. Taylor, R.M. *Roman Builders: A Study in Architectural Process*; Cambridge University Press: Cambridge, UK, 2003; pp. 175–178.
48. Usdowski, E.; Hoefs, J. Oxygen isotope exchange between carbonic acid, bicarbonate, carbonate, and water: A re-examination of the data of McCrea (1950) and an expression for the overall partitioning of oxygen isotopes between the carbonate species and water. *Geochim. Cosmochim. Acta* **1993**, *57*, 3815–3818. [[CrossRef](#)]

